ACS Sustainable Chemistry & Engineering

Research Article

pubs.acs.org/journal/ascecg

Surface-Enhanced Raman Spectroscopy (SERS) Cellular Imaging of Intracellulary Biosynthesized Gold Nanoparticles

Rebecca Halvorson Lahr and Peter J. Vikesland*

Department of Civil and Environmental Engineering and Institute of Critical Technology and Applied Science (ICTAS), Virginia Tech, 418 Durham Hall, Blacksburg, Virginia 24061, United States

Supporting Information

ABSTRACT: Green algae biosynthesize gold nanoparticles (AuNPs) in the presence of dissolved gold, but the precise biosynthesis mechanism remains unclear. Furthermore, few surface-enhanced Raman spectroscopy (SERS) spectra and even fewer SERS cellular images have been collected of intracellularly grown gold nanoparticles, despite the detailed information SERS can provide about nanosurface-associated molecules. In this effort, SERS imaging was used to detect intracellular and extracellular gold nanoparticles biosynthesized by the green algae *Pseudokirchneriella subcapitata* to identify surface-associated biomolecules and to evaluate the nanoparticle biosynthesis mechanism. Three-dimensional SERS spectral maps imaged AuNPs biosynthesized in the presence of 0.005−0.5 mM $HAuCl_4$ over a variety of pH conditions. Algal growth and AuNP biosynthesis were monitored over a 72 h exposure period using UV−vis spectroscopy, electron microscopy, and elemental analysis. Principle component analysis (PCA) and cluster analysis of SERS data demonstrate reproducible trends in the SERS spectral maps and simplify peak identification analyses. SERS cellular images contain peaks consistent with glutathione, *β*-carotene, chlorophyll *a*, hydroxyquinoline, NAD, and proteins such as a reductase enzyme. Each is a biomolecule previously thought to be involved in intracellular AuNP biosynthesis in bacteria and fungi. Little mechanistic study has been previously conducted with green algae. Identification of AuNP surface-associated biomolecules from SERS spectra requires prior knowledge of the system, but peaks not found in the SERS spectra can be used to narrow the list of potential AuNP surface-associated candidate molecules. Continued development of SERS spectral imaging will facilitate noble metal nanoparticle surface analyses to elucidate biosynthesis mechanisms relevant to green synthesis, to monitor nanomaterial function and stability in complex media, and to image AuNPs employed for drug delivery applications.

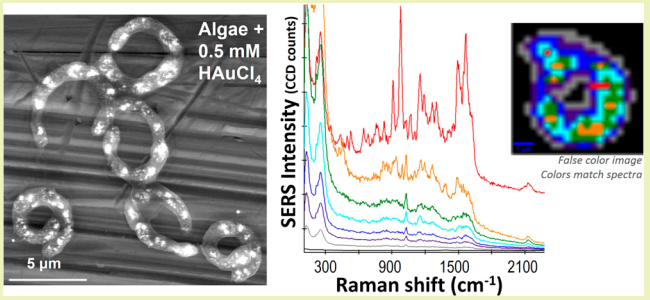

KEYWORDS: *Surface-enhanced Raman spectroscopy (SERS), Cellular imaging, Gold nanoparticles, Intracellular, Extracellular, Biosynthesis, Pseudokirchneriella subcapitata*

INTRODUCTION

Algae, bacteria, and fungi have the capacity to biosynthesize gold nanoparticles (AuNPs) and silver nanoparticles (AgNPs) following dissolved metal uptake.[1−4] There is growing interest in the optimization of these biosynthesis processes for gold recovery from aqueous solutions and for "greener" nanoparticle syntheses.[5,6] Biosorbants for metal recovery require less energy, toxic reagents, or labor to employ than typically used carbon sorption, solvent extraction, ion exchange, or electrodeposition, and metal nanoparticles are a byproduct of this process.[5,7−9] During nanoparticle biosynthesis, dissolved gold ions (Au^{3+}) are reduced to Au^0 intracellularly or extracellularly without the use of acidic or caustic reagents or the input of significant amounts of energy as required for conventional nanoparticle syntheses.[1−3] AuNP bioproduction is attractive as a "green" synthesis method because particles of a wide variety of shapes and sizes can be produced by a single microbial species through growth condition modification (i.e., pH, initial Au concentration, temperature).[10,11] Furthermore, alterations in synthesis rates can be achieved by organism selection. After exposure to Au^{3+}, nanoparticles were observed within minutes for *Plectonema boryanum* and *Anabaena flos-aquae*, but *Calothrix pulvinata* required hours to produce particles.[2,10]

The mechanisms of AuNP and AgNP biosynthesis have been studied for bacteria, fungi, and plants using FT-IR spectroscopy, X-ray photoelectron spectroscopy, zeta potential measurements, enzymatic activity assays, and transmission electron microscopy−electron spectroscopic imaging, but very little work has been done to examine nanoparticle biosynthesis by whole algal cells.[12−15] Furthermore, due to organism specific biochemistries and the tremendous variety of biomolecules that are capable of reducing Au^{3+} to Au^0, the exact mechanisms for intracellular biosynthesis of AuNPs by most microorganisms remain unresolved.[12−15] One theory suggests that the

Special Issue: Sustainable Nanotechnology 2013

Received: February 17, 2014
Revised: April 29, 2014
Published: May 21, 2014

ACS Publications © 2014 American Chemical Society

negatively charged cell wall electrostatically attracts Au^{3+}, that peptidoglycan or enzymes at the cell wall reduce Au^{3+} to Au^0, and following nucleation that nanoparticles are transported through the cell wall.[12,13] Alternate pathways suggested for Au^{3+} bioreduction by bacteria and fungi involve thylakoid membranes, reductase enzymes, and cytochromes.[1,5,12,14] Existing technologies only provide limited information about the biomolecules associated with intracellular nanoparticle surfaces for intact cells.[12−15]

Algal studies documenting intracellular AuNP biosynthesis typically focus solely on metal uptake for recovery from waste streams or omit discussion of the AuNP reduction mechanism.[5,12,15,16] Cyanobacteria lack internal organelles such that the mechanism suggested for blue-green algae may not be entirely applicable to green algae.[1] Incomplete understanding of the mechanisms responsible for uptake of Au^{3+} into algae and its conversion to AuNPs limits optimization of these promising processes. We utilized surface-enhanced Raman spectroscopy (SERS) to systematically probe AuNP biosynthesis in an effort to close this data gap and develop SERS spectral imaging techniques for intracellular analyses. We emphasize that the protocols developed herein for algal imaging are applicable to a variety of cellular environments.

SERS is a vibrational spectroscopic method that provides information about molecules positioned in the vicinity of noble metal nanostructures.[17−19] SERS enables generation of cellular images created by acquisition of hundreds to thousands of Raman spectra across a cell decorated with intracellular or extracellular noble metal nanoparticles. Raman vibrational peaks that correspond to specific biomolecules can be tracked across a single cell, thus documenting the location of biomolecules that associate with the noble metal nanostructures.[20] Such information aids in identification of nanoparticle locations and the delineation of cellular processes.[1] Recently, SERS cellular images collected for a variety of cells have shown the capacity of the method to measure pH in the immediate vicinity of a SERS tag, to mark certain molecular features within a cell, to image cell structures such as hyphae, or to define those biomolecules in the immediate vicinity of a noble metal nanostructure.[20−26] To date, however, few SERS spectra and even fewer SERS cellular images have been collected of intracellularly grown AuNPs, none of which were produced by algal cells.[20,27−30] Thus, SERS cellular imaging is an untapped resource that can answer unsolved questions about nanoparticle biosynthesis. The work described herein enhances our understanding of intracellular AuNP biosynthesis by extending SERS spectral imaging to AuNPs biosynthesized by algal cells, providing chemical imaging to complement electron microscopy.

MATERIALS AND METHODS

ACS reagent grade chemicals were purchased from Fisher Scientific, MP Biomedical, Acros, RICCA Chemical Company, and Electron Microscopy Sciences. $HAuCl_4$ was purchased from MP Biomedical. Phosphate-buffered saline packets (0.01 M PBS; 0.138 M NaCl, 0.0027 M KCl at pH 7.4, 25 °C) were purchased from Sigma (P-3813), and *P. subcapitata* cultures were purchased from Marinco Bioassay Laboratory Aquaculture.

Instrumentation. Absorbance measurements were obtained with a Varian Cary 5000 UV−vis NIR spectrometer and a Biotek μQuant plate reader. An Accumet Basic AB15 Plus electrode from Fisher Scientific was used to monitor pH. Transmission electron microscopy (TEM) micrographs of samples processed and cross-sectioned with a LEICA Ultracut UCT Ultramicrotome were collected using a Zeiss 10CA TEM (60 kV) with an AMT Advantage GR/HR-B CCD camera system and a JEOL JEM 1400 TEM (80 kV) with a Gatan Orius CCD camera controller. Environmental scanning electron microscopy (ESEM) images were recorded with a FEI Quanta 600 FEG operated in ESEM mode with a Peltier stage control kit and a 500 μm gaseous SED detector. The ESEM probe current was continuously adjustable up to 100 nA, and resolution in extended vacuum mode was ≈1.5 nm. One droplet of aqueous-phase sample was placed on the sample holder of the Peltier stage, and the instrument was set at 100% humidity, 6.7 bar pressure, 5 °C, and 20 kV. The sample chamber humidity was then lowered to 80−90% humidity, the highest level at which intact cells were observed. Energy-dispersive X-ray spectroscopy (EDX) was conducted in parallel to ESEM.

Aqueous-phase samples were pipetted onto glass slides, and cells were allowed to settle onto the glass surface before SERS measurements were collected. Cells were examined both fixed and unfixed as well as wet and after drying using a WITec Alpha500R Raman UHTS300 spectrometer, DU 401 BR-DD CCD camera, 785 nm laser, 300 grooves/mm, 100× microscope objectives, and 0.05−50 mW of laser power. Principal component and cluster analyses (Manhattan distance and K-means clustering) were conducted with WITec Project Plus 2.10.3.3 before and after cosmic ray removal, baseline correction, and selection of the 400−2100 cm^{-1} spectral region. Matlab R2013a was used for principal component analysis (PCA) beyond the WITec software capabilities.

Experimental. Algal cultures were grown and handled in accordance with OECD/OCED procedures.[31] Stock cultures were prepared by mixing 50 mL OECD/OCED media with 1 mL *P. subcapitata* culture (Table SI-1, Supporting Information). Stock cultures were grown for 3−6 days until the cell count was $>10^7$ cells/mL as determined with a microscope and hemocytometer or by UV−vis absorbance readings at 440 or 682 nm (corresponding to chlorophyll *a* and carotenoid pigments within algal cells).[31]

Autoclaved 250 mL Erlenmeyer flasks were filled with 50 mL filtered OECD/OCDE media, 1 mL of *P. subcapitata* cells from the stock culture, and 1 mL of an aqueous solution containing the necessary amount of $HAuCl_4$ to make final concentrations of 0.005−0.5 mM $HAuCl_4$. Each concentration was run in triplicate. In parallel, a set of samples containing media and cells were spiked with 1 mL of previously prepared 40 nm citrate stabilized AuNPs.[32] Prepared flasks were capped with autoclaved cotton balls and incubated at 23 °C on a shaker table under fluorescent lighting for the duration of the incubation. Samples were removed from each flask for analysis at approximately 12 h increments. The volume of solution in each flask did not fall below 40 mL during the 72 h incubation. Visual descriptions with and without microscope and plate reader measurements at 300, 440, 520, 633, 682, and 785 nm were collected every 12 h. Raman scans, optical images, and ESEM images were recorded every 24 h. In addition, TEM images and 250−800 nm UV−vis scans were collected at 72 h. After 72 h, the flask contents were filtered through a 0.2 μm polycarbonate Millipore membrane filter and placed in a 2 mL centrifuge tube containing 2.5% glutaraldehyde in 0.01 M PBS buffer for analyses that could not be conducted immediately.

pH Control. A set of pH regulated samples were setup, incubated, and monitored as previously described; however, pH was adjusted using 0.1 N NaOH or HCl before the algae was added to the flask containing media and $HAuCl_4$ solution.[3] pH was measured initially and every 12 hours throughout the incubation. Samples for which pH was regulated include controls of algae in growth media, media controls containing 0.5 mM $HAuCl_4$ without algae, and algae in growth media containing 0.5 or 0.15 mM $HAuCl_4$, all of which were examined at both pH 3 and pH 8.

TEM Cross-Sectioning. After filtration and fixation as described previously, cells were washed in PBS, stained with 1% OsO_4, pelleted in agar, and suspended in Spurr's resin (Supporting Information contains additional details).[33−35] Cross sections were cut, placed on grids, and examined by TEM. ImageJ (NIH, Ver. 1.46) was used to measure AuNP sizes from images. Averages and standard deviations were computed from at least 50 AuNPs or all the AuNPs of the specified size and location across at least five typical cells.

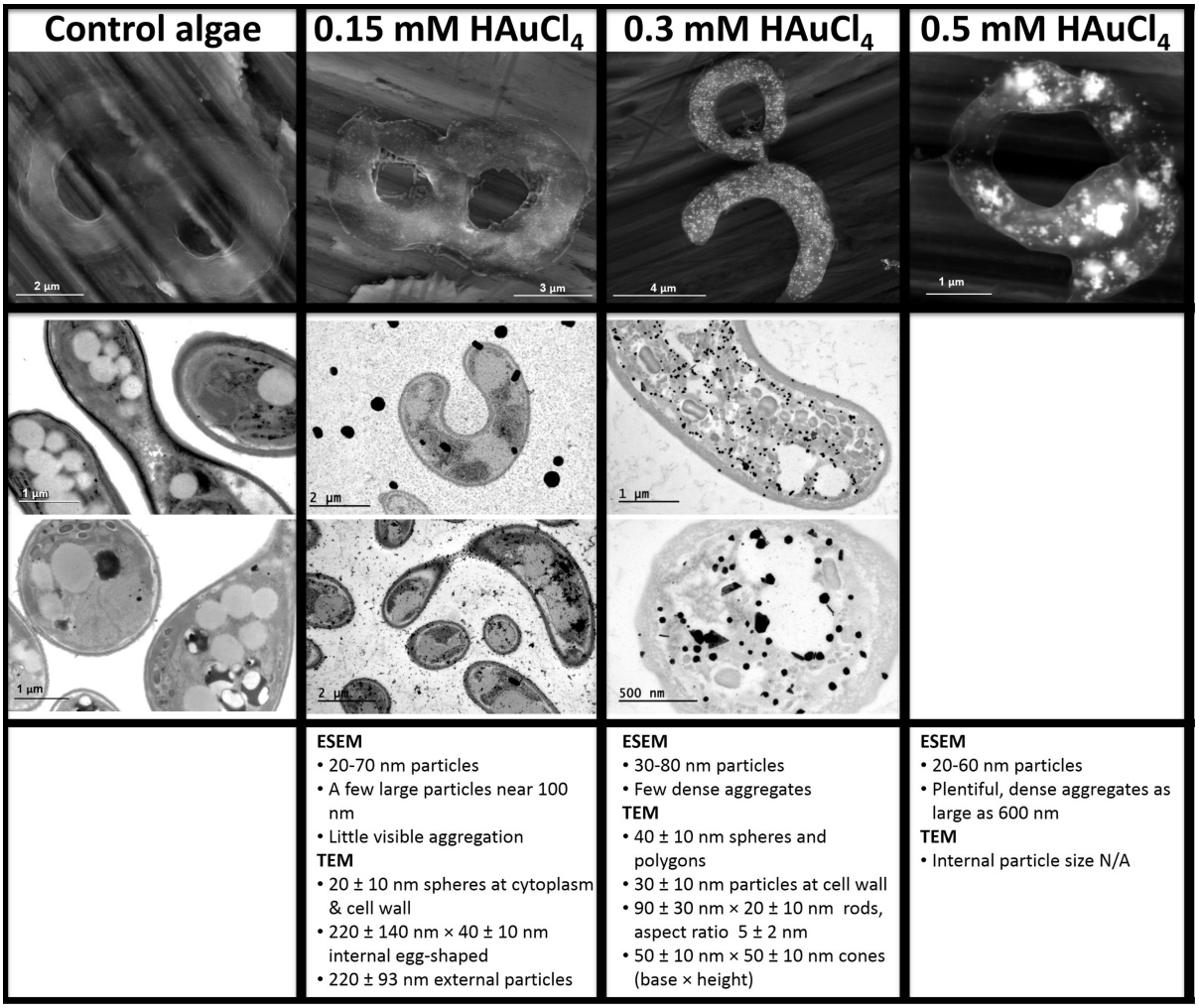

Figure 1. ESEM whole cell (first row) and TEM cross-sectional images (second row) were collected for *P. subcapitata* incubated with 0−0.5 mM $HAuCl_4$ for 72 h, filtered through a 0.2 μm filter, and fixed with 2.5% glutaraldehyde. Electron-dense gold is displayed as white in ESEM images and black in TEM images. Staining with osmium tetroxide before cross-sectioning for TEM analysis identifies unsaturated lipids (i.e., cell and organelle membranes).[38] The third row summarizes the characteristics of the AuNPs for each condition. Control cells were imaged at pH 8, 0.15 mM $HAuCl_4$ at pH 7, and 0.3−0.5 mM $HAuCl_4$ at pH 3. Histograms of particle size are included in Figure SI-4 of the Supporting Information. (Note: No TEM images for the 0.5 mM $HAuCl_4$ incubation were obtained.).

RESULTS AND DISCUSSION

On the basis of cell counts, visual observations, and absorbance measurements at 682 nm, exposure to 0.005−0.04 mM $HAuCl_4$ had little effect on *P. subcapitata* growth rates, but growth halted in 0.08−0.5 mM $HAuCl_4$ (Figure SI-1, Supporting Information). After a 72 h incubation, algal cells in control samples and incubations with less than 0.08 mM $HAuCl_4$ reached the stationary phase. The decrease in pH due to the $HAuCl_4$ addition was not the cause of cell death for initial $HAuCl_4$ concentrations greater than 0.08 mM; cell growth was also inhibited in 0.15 and 0.5 mM $HAuCl_4$ samples fixed at pH 8.

AuNPs Growth. ESEM images, collected for samples removed directly from incubation flasks every 24 h and every 72 h for samples that were filtered and fixed in glutaraldehyde, demonstrate AuNP biosynthesis but cannot differentiate intracellular AuNPs from AuNPs associated with the algal surface (Figure 1). AuNPs are visible within 24 h of incubation in the 0.5 mM $HAuCl_4$ sample, but longer incubation periods were required for lower initial gold concentrations. TEM cross-sectional images, obtained after 72 h, confirm intracellular AuNP production and facilitate particle sizing (Figure 1). EDX further affirms that the nanoparticles are AuNPs (Figure SI-2, Supporting Information).

AuNPs exhibit characteristic absorption bands (localized surface plasmon resonances, LSPR) whose location and magnitude are defined by the size of the nanoparticle and its local chemical environment. In water, the LSPR wavelength for discrete 15 nm gold spheres occurs at 520 nm, but as the diameter increases to 99 nm, the wavelength red-shifts to 575 nm.[36] Only two LSPR bands were observed by UV−vis spectroscopy in any of the incubation flasks. A LSPR band at 524 nm was exhibited by samples spiked with presynthesized 40 nm citrate AuNPs, and another LSPR band at 567 nm was identified in incubations containing 0.15 mM $HAuCl_4$ at pH 3 (Figure SI-3, Supporting Information). A UV−vis peak was only observed for the 0.15 mM $HAuCl_4$ condition at pH 3, despite confirmation of AuNPs presence by electron microscopy and EDX in other algal incubation flasks containing $HAuCl_4$. At the initial algal concentration of 2×10^5 cells/mL, the absorbance of chlorophyll *a*, carotenoid, and intracellular AuNPs were not detectable by UV−vis spectroscopy, even for

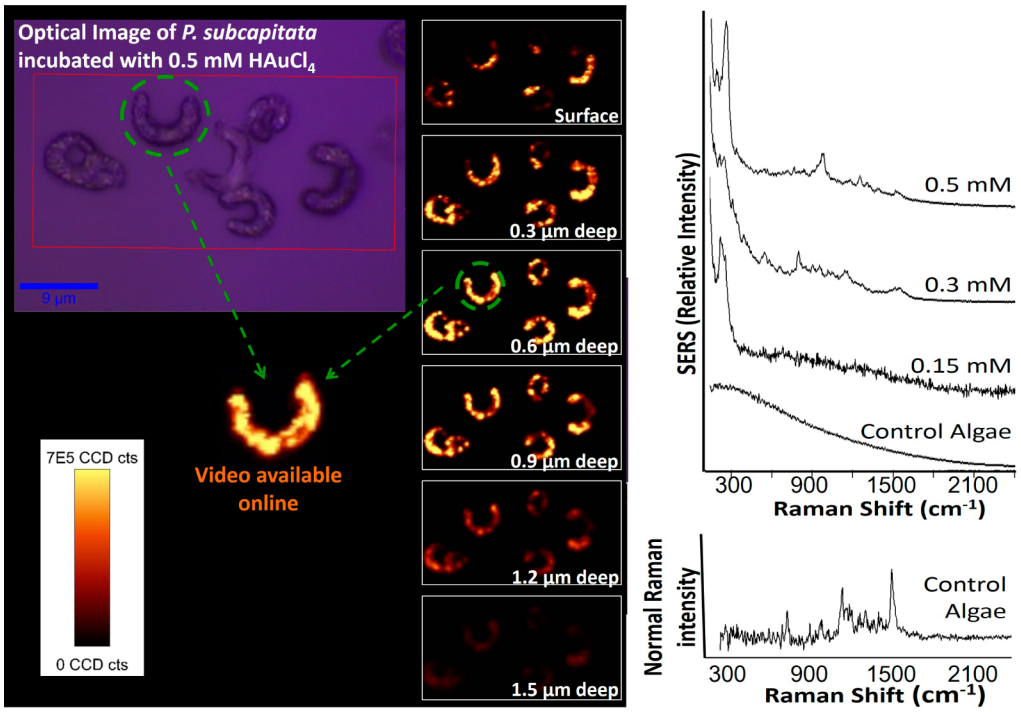

Figure 2. SERS signals originate from within the algal cell rather than at the surface, as demonstrated by stacked *x,y,z* SERS spectral maps. Three spectra per μm were collected, and the overall spectral intensity of each spectrum was used to convert 7560 spectra into a single *x,y* image for each depth. High numbers of CCD counts (yellow) are observed by the instrument detector only inside of the cells. A video demonstrating the particle locations in 3D space within the indicated cell is available electronically. SERS spectra for the cells in each spectral map were averaged and are shown before baseline correction on arbitrary scales for viewing ease. The normal Raman spectrum was collected with a higher sample concentration, laser power, and acquisition time for comparison with SERS spectra. (Table SI-2 of the Supporting Information contains specific Raman spectrometer parameters for each condition.).

control algae that produced significant chlorophyll *a* and carotenoid absorbances after 72 h (Figures SI-1 and SI-3, Supporting Information). LSPR absorbances of intracellularly biosynthesized AuNPs have been observed by Focsan et al. and others at higher cell counts.[1,37] Therefore, it is assumed that low cell counts and the intracellular nature of the AuNPs result in few UV−vis detectable AuNPs.

Raman and SERS Characterization of Algal Cells. The growth and aggregation of biosynthesized AuNPs results in enhanced Raman spectral intensity. In the presence of AuNPs, SERS spectra are observed using 1% of the laser power and 10% of the acquisition time required for normal Raman cellular imaging (Figure 2 and Figure SI-5, Supporting Information). Control cells grown without $HAuCl_4$ display low intensity fluorescence signals without defined Raman spectral peaks when probed at low laser powers and short acquisition times. AuNPs have the ability to quench fluorescence, and this property combined with the enhancement effect allowed SERS signals to be visible for cells incubated with $HAuCl_4$.[19] A SERS spectrum is only obtained when the LSPR band of the noble metal nanostructure overlaps with the Raman laser wavelength.[18,19] Therefore, for experiments conducted with a 785 nm Raman laser, AuNPs must either be large (>40−50 nm) or have many particle junctions (overlapping AuNP electromagnetic fields) to produce a SERS effect.[18] On the basis of the observed size of AuNPs in the collected TEM and SEM images, it would appear that the latter mechanism is primarily at play in this system. Importantly, the 785 nm laser selectively probes those biomolecules associated with larger particles or aggregates. The collected SERS spectra represent a snapshot chemical image of the biomolecules associated with these larger AuNPs or aggregate surfaces during equilibrium, aggregation, or growth, but not nucleation. Had a 514 nm laser been applied to the same samples, smaller particles or aggregates would have enhanced the Raman spectra, thus resulting in identification of biomolecules associated with those smaller nanoparticles.

Three-dimensional Raman scans demonstrate that the majority of the SERS signal originates from within the algal cells rather than simply from their surface (Figure 2 and video, Supporting Information). The spectra observed within the cells exhibit spatial variability caused by the transient nature of SERS, association of AuNPs with a variety of biomolecules in a variety of orientations in the cell, variety of AuNP sizes and shapes, and SERS hot spots produced at the junctions and corners of particles where electromagnetic fields produced by the localized surface plasmon bands of the nanostructures overlap.[18,19] SERS hot spots are operationally defined herein as a location that produces a spectrum containing unique peaks that are at least 10× more intense over 400−2200 cm^{-1} than the typical spectrum for that cell, reflecting junctions between nanoparticles or a strong binding event with a biomolecule that is only observed once. Identifying sources of molecular vibrations that produce intracellular SERS signals in complex biological systems is complicated and requires significant amounts of data as indicated by Prusinkiewicz et al.;[24] principal component analysis (PCA) and cluster analysis were applied to find statistically relevant patterns within the SERS spectral maps.

Data Reduction. PCA is a statistical method often used to emphasize variations in large data sets, rather than the variables that remain constant.[39] A new combination of the original variables, known as principal components (PCs), is created to

order and highlight the aspects of the data set that are unique. The percentage of variability in the data described by each PC is computed, and the PCs are ordered by the amount of variability explained by each PC, with the first PC being the most significant. For a single algal cell incubated with 0.5 mM $HAuCl_4$ at pH 3, one PC explained 80−95% of the variability among spectra. The loadings for the first PC highlighted similar peaks for each cell, with cells incubated under similar conditions typically sharing more similarities than those of cells incubated under different conditions (Figure SI-6, Supporting Information).

Cluster analysis partitions spectra within a SERS spectral image into a predefined number of groups of similar spectra.[39] In cluster analysis with two clusters defined (chosen based on the PCA results), the crescent-shaped algal cell can be differentiated from the background. If the *P. subcapitata* cell SERS spectra are divided into additional clusters, a single spectrum of varying intensity is observed across the majority of each cell with periodic signal hotspots that are unique and not reproducible (Figure 3). The most intense cluster for each cell

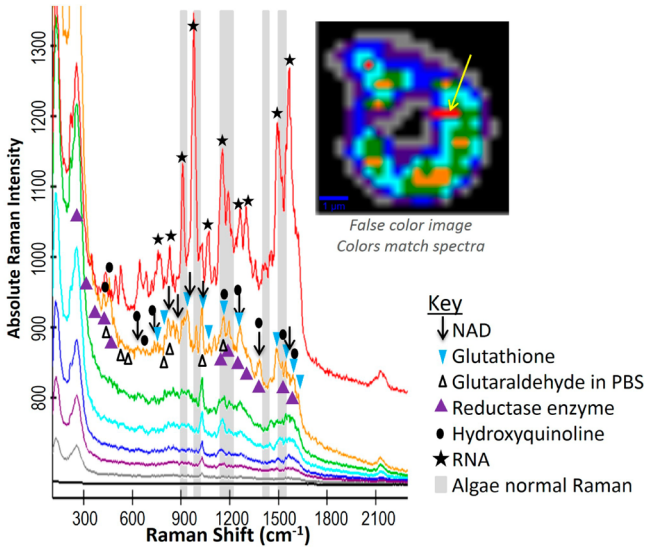

Figure 3. Cluster analysis of a cell incubated with an initial concentration of 0.5 mM $HAuCl_4$ at pH 3 in growth media demonstrates the intracellular nature of the biosynthesized AuNPs. Each spectrum corresponds to the location indicated by the corresponding color in the Raman spectral map. A spot producing more intense and different peaks from those observed throughout the rest of the cell is indicated by the yellow arrow. Absolute SERS intensities demonstrate the strength of each spectrum and the extent of the signal enhancement. The red spectrum was shifted upward by 100 CCD counts for viewing ease. Biomolecule spectra are referenced in Table SI-3 of the Supporting Information.[40−58]

typically matched the peaks highlighted by the loadings of the first PC (Figures SI-6 and SI-7, Supporting Information), demonstrating an agreement between the PCA and cluster analysis, reproducible nature of spectra across an algal cell, and significance of the SERS peaks displayed by the algae.

The reproducibility of SERS spectra for a given condition was evaluated by conducting PCA of the average cluster analysis spectra given in Figure SI-7 of the Supporting Information (an average spectrum for each of 14 separate cells, 3−4 for each incubation condition). Each condition was arbitrarily assigned a number one through four. A linear regression was then developed to describe the trend between the first few PC scores and the incubation condition number. Ten PCs were required in the regression to mathematically predict the incubation condition number from the PC scores after omitting the SERS hotspot spectra (Figures SI-6, SI-7, and SI-8, Supporting Information). The ability of a PC regression to mathematically predict the initial incubation condition for all 14 spectra suggests that two spectra from different incubation conditions are consistently unique enough for the model to differentiate them. Thus, SERS spectra were reproducible across a single algal incubation condition. The most common SERS vibrations highlighted by cluster analysis and PCA were further studied to identify their origins.

AuNP Surface-Associated Biomolecules. Zeiri and Sengupta determined that silver nanoparticles extracellularly synthesized by *E. coli* reproducibly display a spectrum similar to that of flavin adenine dinucleotide (FAD) due to the high affinity of this molecule for the nanoparticle surface.[59,60] *P. subcapitata* biosynthesized AuNPs do not follow such a simple trend; nonetheless, PCA and cluster analyses provide evidence of patterns. Algal SERS spectra were compared to spectra of basic biomolecules as well as biomolecules thought to take part in the reduction or stabilization of biosynthesized AuNPs (i.e., carotenoids, chlorophyll, polysaccharides, hexosamines, tannins, amino acids, and quinones).[5,6,9,12,40−58,61] Normal Raman spectra are generally strongest for nonpolar functional groups, but the chemical enhancement mechanism for SERS distorts this trend. The SERS spectrum of a molecule in contact with a AuNP will be enhanced by 10−100× in addition to the enhancement expected from the biomolecule's position within the electromagnetic field generated about the AuNP due to laser irradiation.[18] Therefore, the strongest peaks are hypothesized to be generated by biomolecules associated with the AuNP surface.

SERS spectra for all $HAuCl_4$ incubation conditions contained a very strong peak at 240−275 cm^{-1} due to vibrations between Au^0 and Cl, S, N, or C, reaffirming that SERS spectra document biomolecules at AuNP surfaces.[62−65] Peaks at 1030−1034, 1157−1166, 1244−1278, 1544−1554, 1584−1591, and 2125−2146 cm^{-1} were also common, documenting vibrations also displayed by nicotinamide adenine dinucleotide (NAD), β-carotene, glutathione, hydroxyquinoline, chlorophyll, and proteins (Figure 4, Table SI-4, Supporting Information). As also encountered by Prusinkiewicz et al., SERS vibrations associated with several of these biomolecules overlap, and the tendency for SERS to distort respective peak ratios due to orientation of the molecule about the AuNP surface hinders precise differentiation of all peaks. However, the ability of SERS to rapidly narrow down the list of biomolecules that are associated closely (within 4 nm) with the AuNP surface is a significant finding to complement FT-IR, X-ray spectroscopies, assays of cell function, and in vitro syntheses for the determination of mechanisms responsible for AuNP biosynthesis. Peaks that are not found in the SERS spectra for any condition are likely not interacting closely with nanoparticle surfaces, thus ruling out the glutaraldehyde fixing agent, saccharides, FAD, lipids, DNA, and other AuNP associations. Furthermore, PCA highlighted the peaks that caused the most variation within the data set, thus simplifying peak identifications and differentiating overlapping signals.

The loadings of the top PCs required for prediction of incubation conditions were plotted against various biomolecule spectra (Figure 5). The loadings of PC1 and PC2 contain

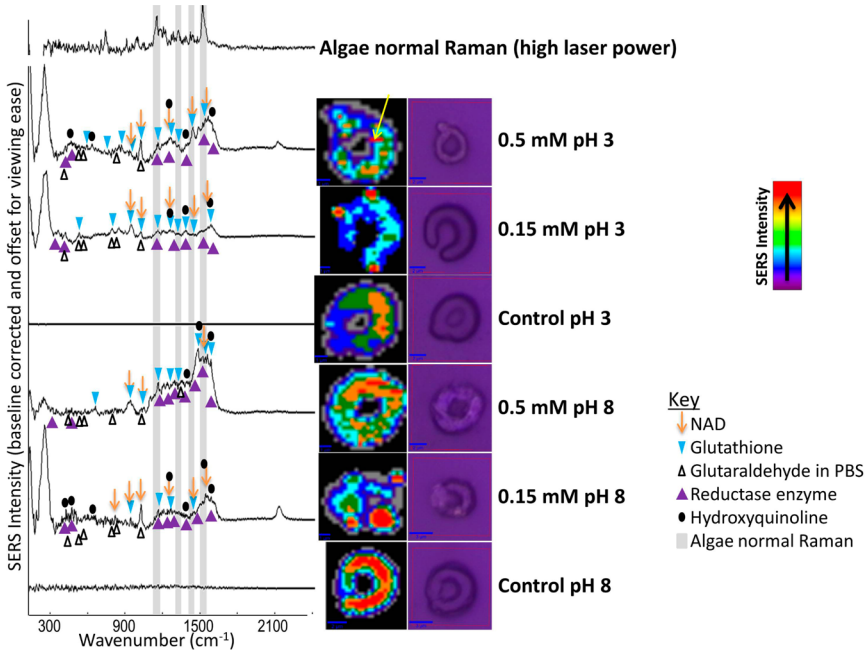

Figure 4. Cluster analysis of pH controlled algae incubations. Optical images (purple) and SERS spectral maps (false color images) are shown alongside an average spectrum taken of the most intense cluster for three distinct cells at the indicated condition. The nonlinear image intensity scale is not normalized for comparison across the different conditions; images for control algae are produced by fluorescence rather than Raman signal. SERS hotspots (yellow arrow, 0.5 mM pH 3) were considered as a separate entity and the next most intense cluster was used for averaging. Variability was not observed in the control cell SERS spectral images, so data from a single cell are shown. To improve the signal from that displayed in Figure SI-4 of the Supporting Information, the laser power was reduced to <0.05 mW and acquisition time was increased (Table SI-2, Supporting Information). Biomolecule spectra are referenced in Table SI-3 of the Supporting Information.[40−58]

features observed in β-carotene and chlorophyll *a*. The loadings of PCs 3−6 display peaks common to glutathione, with protein peaks around 1100−1375, 1650, and 1445 cm^{-1} also visible in PC5 and PC6.[41] Nonspecific orientation of a biomolecule at AuNP surfaces would cause the PC loadings to highlight variations of the biomolecule's spectrum across multiple PCs.[66] Thus, the main differences in surface coatings of the AuNPs produced at the various incubation conditions appear to be correlated with glutathione, β-carotene, chlorophyll *a*, and possibly proteins.

Mechanistic Interpretation of SERS Spectra. PCA highlights variation in data sets rather than peaks that remain constant; comparison with the cluster analysis results is valuable for identifying peaks that are constant. From peak identifications, it is clear that glutathione plays a role as a metal binding peptide that stabilizes AuNPs. The SERS data supports two potential mechanisms proposed elsewhere for bacteria and fungi, including chlorophyll *a* and β-carotene as electron sources for AuNP reduction as seen in cyanobacteria or hydroxyquinoline and NADH may transfer electrons to facilitate function of a reductase enzyme as observed in fungi.[1,61,67,68] At the high $HAuCl_4$ concentrations discussed here, it is likely that more than one mechanism is responsible for the variety of AuNP shapes and sizes, with initial conditions influencing the pathways employed.

Chlorophyll a and Carotenoids. Algal SERS spectra for all conditions maintain a set of peaks similar to those in the normal Raman spectrum of the algae (primary peaks highlighted in gray in Figures 3 and 4). This observation is interesting because SERS spectra are collected with a much lower laser power (<0.05 mW SERS versus >40 mW normal Raman), and no Raman or SERS signals were obtained for algae without AuNPs at <0.05 mW of laser power. This finding suggests that the same biomolecules that are responsible for producing the algal normal Raman spectrum are interacting within 4 nm of the AuNPs.[19] The peaks in the normal Raman algal spectrum are identified as chlorophyll *a* and β-carotene, identical to that observed by Wood et al. (Figure 5). Therefore, chlorophyll *a* and β-carotene interact with the biosynthesized AuNPs. Such a finding is not surprising. Pigments such as β-carotene are often produced to protect algal cells against photooxidants.[61,69] AuNPs biosynthesized by cyanobacteria are found to associate with thylakoids where photosynthetic electrons are employed for Au^{3+} reduction.[1] AuNPs have been produced by chloroplasts extracted from the *Trifolium* leaf,[70] and Barazzouk et al. successfully employed AuNP to photoprotect chlorophyll because of its affinity to form a self-assembled monolayer on AuNP.[71] SERS spectra consistently display a peak at 2137 cm^{-1} that reflects C−N vibrations at a gold surface.[63,64] The detector on the Raman spectrometer employed for this analysis is less sensitive to high wavenumber peaks such as 2137 cm^{-1} with the 785 nm laser setup (indicated by instrument specifications and experimental verification). Although the peak at 2137 cm^{-1} is weak in some of the algae samples, its intensity in relation to the minimal sulfur SERS peaks at 630−670 and 700−745 cm^{-1} suggest that a nitrogen atom rather than a sulfur atom most frequently coordinates with the AuNP, a finding supported by Mukherjee et al.[13,41,63,72]

Glutathione and Phytochelatin. Glutathione is both a precursor of phytochelatin and a metal binding compound thought to help transport metals to polyphosphate granules, the cytoplasmic membrane, or vacuoles.[68] Phytochelatin is an oligomer of glutathione produced intracellularly by *P. subcapitata* and other algae in the presence of Cd, Zn, Cu, Ag, Hg, and Pb to bind metals for detoxification; this molecule

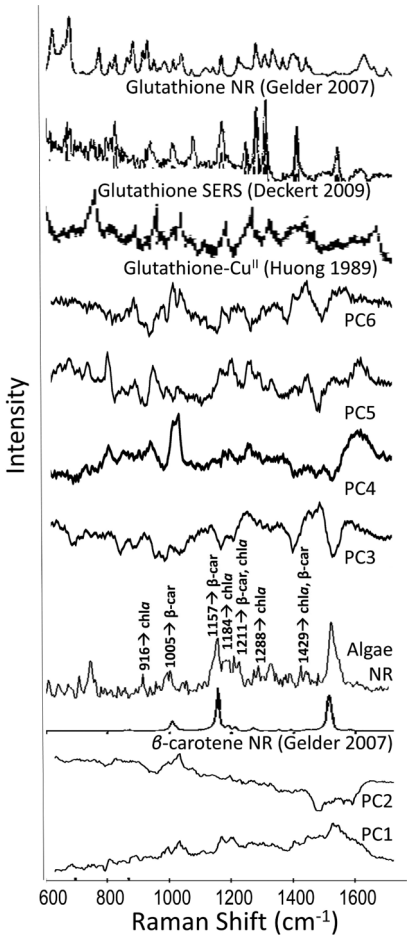

Figure 5. Comparison of PC loadings with normal Raman (NR) and SERS spectra of the algae, β-carotene, and glutathione.[40,50,51] Algae NR peak identifications are adapted from Wood et al.[58] Additional PC loadings are included in Figure SI-7 of the Supporting Information.

has been employed experimentally to stabilize particles formed by a reductase enzyme.[61,67,68] SERS data suggests glutathione or phytochelatin is also produced by *P. subcapitata* in the presence of $HAuCl_4$. Ma et al. determined that surface area rather than concentration dictates the overall toxicity of a prefabricated metal NP to an organism.[73] Phytochelatin levels have been observed at an order of magnitude lower than that of the heavy metal;[68] this is expected for a molecule used as a surface coating for small nanoparticles rather than an agent used to bind each metal ion separately.

Other Biomolecules (Supporting Information contains additional discussion). The rare occurrence of the RNA SERS spectra, only in SERS hotspots, suggests that although RNA will readily associate with AuNP surfaces, it is not the primary reducing or stabilizing agent within the *P. subcapitata* cells (Figure 3). Enzymes produce complex Raman spectra with many overlapping peaks, especially reflecting amide bonds at 1100−1375 and 1623 cm^{-1}, CH_2 bending at 1445 cm^{-1}, and phenylalanine at 1004 cm^{-1}, with various other specific amino acid peaks.[41] SERS spectra of proteins are even more complex unless binding to AuNPs occurs in a consistent conformation. Protein peaks are reflected in the algal SERS spectra and PC loadings, but specific protein identification requires additional study (Figure 5).

The strength of the 2137 cm^{-1} C−N SERS peak in comparison to the weaker C−S peaks that periodically appear at 630−670 and 700−745 cm^{-1} may be surprising considering the known affinity of Au for S.[41,63,64,72,74,75] Mukherjee et al. also observed linkages of AgNP with nitrogen atoms rather than sulfur in a single Raman spectrum of AgNP produced using cell-free aqueous filtrate from *Trichoderma asperellum*.[72] AuNPs biosynthesized by chloroplasts and examined by FTIR by Zhang et al. were determined to be capped by glutathione bound via free amine groups.[70] Reduced glutathione has both thiol and amide groups for coordination with Au^0. The oxidation of glutathione results in a disulfide bridge between the thiols of two glutathiones,[50] leaving the sulfur atoms more sterically hindered than the nitrogen atoms. Therefore, if glutathione were indirectly involved in the reduction of Au^{3+} to Au^0, linkage of glutathione to AuNPs through nitrogen atoms would not be unexpected.

Impact of Initial Conditions on AuNP Biosynthesis. Algal cells respond uniquely to each incubation condition, as verified by TEM, SEM, UV−vis, and SERS spectral imaging data showing dissimilar particles for each condition, a finding also observed elsewhere.[9,76] SERS spectral maps of the 0.15 mM $HAuCl_4$ samples at pH 3 displayed large islands of SERS signal that did not directly correlate with the cells shown in the simultaneously collected optical images (Figure 4). This result, along with the observed UV−vis LSPR absorbance, supports the hypothesis that a significant portion of the SERS active AuNPs in the 0.15 mM $HAuCl_4$ samples at pH 3 were extracellular. At pH 8 for the same initial concentration, the SERS signal also does not spatially correlate with the algal cells, indicating external particles; however, the dimensions of the SERS signal spots are inconsistently shaped and sized, a finding contrary to all other incubation conditions examined. The polydispersity of external AuNPs for the 0.15 mM $HAuCl_4$ sample at pH 8 may explain the lack of a UV−vis LSPR absorbance peak (i.e., an insufficient concentration of any single particle size to produce a detectable LSPR band). At the higher $HAuCl_4$ concentration (0.5 mM), the SERS spectral images closely match the optical images because the SERS active AuNPs are intracellular (Figure 4). This finding is also apparent in the 3D SERS cellular images available online. The intracellular AuNPs at 0.5 mM $HAuCl_4$ grew large enough during the 72 h incubation for the LSPR bands to occur near the 785 nm Raman laser wavelength, thus producing the observed SERS signals. SERS chemically images AuNPs within cells with minimal user effort to complement electron microscopy images.

Peak identifications for the pH-controlled incubations at 0.5 mM and 0.15 mM $HAuCl_4$ are shown for the most intense clusters averaged for three cells, excluding SERS (Figure 4). Similar peaks were typically observed for all conditions, with intensity variability. The 0.15 mM $HAuCl_4$ cells at pH 3 do not have as high of a contribution of peaks from chlorophyll *a* or β-carotene as the other incubations (Figures 4 and 5). This finding is logical considering the extracellular nature of the particles. Cell lysis would be required before extracellular particles would be formed by or come into contact with chloroplasts. The intracellular nature of the AuNPs formed at 0.5 mM $HAuCl_4$ also explains the higher intensity of peaks at 1200−1300 and 1500−1600 cm^{-1}, attributed to amide vibrations of proteins, glutathione, or phytochelatin for the 0.5 mM $HAuCl_4$ samples (Figures 4 and 5).[41] The intracellular environment typically has a higher concentration of proteins, and phytochelatin is produced intracellularly.

CONCLUSIONS AND FUTURE OUTLOOK

The common, harmless, simple to grow, green algae *P. subcapitata* produces AuNP in the presence of $HAuCl_4$, scavenging the noble metal and producing AuNP that associate with algal cells. This first SERS cellular imaging study of intracellularly biosynthesized AuNP produced by green algae demonstrates the AuNP biosynthesis capabilities of *P. subcapitata* as well as the utility of SERS spectral imaging for documenting the location, size, surface-coating, and local molecular environment of intracellular and extracellular noble metal nanostructures. Sample preparation is much more rapid and less invasive than electron microscopy, and chemical images provide complementary data to existing nanoparticle characterization techniques. The intracellular or extracellular nature of AuNP is immediately apparent via SERS cellular imaging, without the necessity of invasive multi-day cross-sectioning for TEM analysis. Strategic Raman laser selection targets the analysis to specific nanoparticle sizes.

Three-dimensional SERS cellular imaging produces large quantities of data within minutes, such that PCA or cluster analysis are necessary to quickly infer the most important aspects of the large data sets. SERS spectra reflected vibrations common to glutathione, β-carotene, NAD+, hydroxyquinolone, chlorophyll, and proteins rather than the glutaraldehyde fixing agent, saccharides, FAD, lipids, DNA, and others. Peaks varied among incubations containing different initial $HAuCl_4$ concentrations and pH, but SERS spectra were reproducible across each single incubation condition. SERS will continue to be a valuable tool for confirming suspected AuNP surface-associated molecule identities. Understanding the interactions between biosynthesized noble metal nanomaterials and their local environment will improve overall understanding of these systems such that they may be engineered to best fit the needs of society.

ASSOCIATED CONTENT

Supporting Information

Specific details regarding algal growth media, TEM cross-sectioning procedures, confirmation of algal and nanoparticle growth, Raman spectrometer settings, PCA results, and discussion of biomolecules potentially correlated with Raman spectra. This material is available free of charge via the Internet at http://pubs.acs.org.

AUTHOR INFORMATION

Corresponding Author

*E-mail: pvikes@vt.edu.

Notes

The authors declare no competing financial interest.

ACKNOWLEDGMENTS

We thank Dr. Weinan Leng for his insights regarding the WITec Alpha 500R, Matt Chan for assistance with *P. subcapitata*, Kathy Lowe for sample prep and TEM expertise, and Steve McCartney for ESEM advice and training. This work was supported by an Abel Wolman graduate research fellowship to R.H.L. from the American Water Works Association (AWWA) and research grants from the Center for the Environmental Implications of Nanotechnology (CEINT) and the Virginia Tech Institute for Critical Technology and Applied Science (ICTAS).

REFERENCES

(1) Focsan, M.; Ardelean, I. I.; Craciun, C.; Astilean, S. Interplay between gold nanoparticle biosynthesis and metabolic activity of cyanobacterium *Synechocystis* sp. PCC 6803. *Nanotechnology* **2011**, *22* (48), 485101.

(2) Lengke, M. F.; Ravel, B.; Fleet, M. E.; Wanger, G.; Gordon, R. A.; Southam, G. Mechanisms of gold bioaccumulation by filamentous cyanobacteria from gold(III)−chloride complex. *Environ. Sci. Technol.* **2006**, *40* (20), 6304−6309.

(3) Parial, D.; Patra, H.; Roychoudhury, P.; Dasgupta, A.; Pal, R. Gold nanorod production by cyanobacteria—a green chemistry approach. *J. Appl. Phycol.* **2012**, *24* (1), 55−60.

(4) Lengke, M. F.; Fleet, M. E.; Southam, G. Morphology of gold nanoparticles synthesized by filamentous cyanobacteria from gold(I)−thiosulfate and gold(III)−chloride complexes. *Langmuir* **2006**, *22* (6), 2780−2787.

(5) Das, N. Recovery of precious metals through biosorption—A review. *Hydrometallurgy* **2010**, *103* (1−4), 180−189.

(6) Mata, Y. N.; Torres, E.; Blázquez, M. L.; Ballester, A.; González, F.; Muñoz, J. A. Gold(III) biosorption and bioreduction with the brown alga *Fucus vesiculosus*. *J. Hazard. Mater.* **2009**, *166* (2−3), 612−618.

(7) Kuyucak, N. Feasibility of Biosorbant Applications. In *Biosorption of Heavy Metals*; Volesky, B., Ed.; CRC Press: Boca Raton, 1997; pp 371−378.

(8) Korbekandi, H.; Iravani, S.; Abbasi, S. Production of nanoparticles using organisms. *Crit. Rev. Biotechnol.* **2009**, *29* (4), 279−306.

(9) Vijayaraghavan, K.; Mahadevan, A.; Sathishkumar, M.; Pavagadhi, S.; Balasubramanian, R. Biosynthesis of Au(0) from Au(III) via biosorption and bioreduction using brown marine alga *Turbinaria conoides*. *Chem. Eng. J.* **2011**, *167* (1), 223−227.

(10) Brayner, R.; Barberousse, H.; Hemadi, M.; Djedjat, C.; Yéprémian, C.; Coradin, T.; Livage, J.; Fiévet, F.; Couté, A. Cyanobacteria as bioreactors for the synthesis of Au, Ag, Pd, and Pt nanoparticles via an enzyme-mediated route. *J. Nanosci. Nanotechnol.* **2007**, *7* (8), 2696−2708.

(11) Konishi, Y.; Tsukiyama, T.; Tachimi, T.; Saitoh, N.; Nomura, T.; Nagamine, S. Microbial deposition of gold nanoparticles by the metal-reducing bacterium *Shewanella algae*. *Electrochim. Acta* **2007**, *53* (1), 186−192.

(12) Durán, N.; Marcato, P. D.; Durán, M.; Yadav, A.; Gade, A.; Rai, M. Mechanistic aspects in the biogenic synthesis of extracellular metal nanoparticles by peptides, bacteria, fungi, and plants. *Appl. Microbiol. Biotechnol.* **2011**, *90*, 1609−1624.

(13) Rai, M. *Metal Nanoparticles in Microbiology*; Springer: Berlin, 2011.

(14) Das, S. K.; Liang, J.; Schmidt, M.; Laffir, F.; Marsili, E. Biomineralization mechanism of gold by zygomycete fungi *Rhizopous oryzae*. *ACS Nano* **2012**, *6* (7), 6165−6173.

(15) Quester, K.; Avalos-Borja, M.; Castro-Longoria, E. Biosynthesis and microscopic study of metallic nanoparticles. *Micron* **2013**, *54*−*55* (0), 1−27.

(16) Ting, Y. P.; Teo, W. K.; Soh, C. Y. Gold uptake by *Chlorella vulgaris*. *J. Appl. Phycol.* **1995**, *7*, 97−100.

(17) Fleischmann, M.; Hendra, P. J.; McQuillan, A. J. Raman spectra of pyridine adsorbed at a silver electrode. *Chem. Phys. Lett.* **1974**, *26*, 163−166.

(18) Halvorson, R. A.; Vikesland, P. J. Surface-enhanced Raman spectroscopy (SERS) for environmental analyses. *Environ. Sci. Technol.* **2010**, *44* (20), 7749−7755.

(19) Haynes, C. L.; McFarland, A. D.; Van Duyne, R. P. Surface-enhanced Raman spectroscopy. *Anal. Chem.* **2005**, *77* (17), 338A−246A.

(20) Ravindranath, S. P.; Henne, K. L.; Thompson, D. K.; Irudayaraj, J. Raman chemical imaging of chromate reduction sites in a single bacterium using intracellularly grown gold nanoislands. *ACS Nano* **2011**, *5* (6), 4729−4736.

(21) McAughtrie, S.; Lau, K.; Faulds, K.; Graham, D. 3D Optical imaging of multiple SERS nanotags in cells. *Chem. Sci.* **2013**, *4* (9), 3566−3572.
(22) Kneipp, J.; Kneipp, H.; Wittig, B.; Kneipp, K. Novel optical nanosensors for probing and imaging live cells. *Nanomed. Nanotechnol. Biol. Med.* **2010**, *6* (2), 214−226.
(23) Abbas, A.; Josefson, M.; Nylund, G. M.; Pavia, H.; Abrahamsson, K. Chemical images of marine bio-active compounds by surface enhanced Raman spectroscopy and transposed orthogonal partial least squares (t-opls). *Anal. Chim. Acta* **2012**, *737* (0), 37−44.
(24) Prusinkiewicz, M. A.; Farazkhorasani, F.; Dynes, J. J.; Wang, J.; Gough, K. M.; Kaminskyj, S. G. Proof-of-principle for SERS imaging of *Aspergillus nidulans* hyphae using in vivo synthesis of gold nanoparticles. *Analyst* **2012**, *137* (21), 4934−42.
(25) Ando, J.; Yano, T.-a.; Fujita, K.; Kawata, S. Metal nanoparticles for nano-imaging and nano-analysis. *Phys. Chem. Chem. Phys.* **2013**, *15* (33), 13713−13722.
(26) Vitol, E. A.; Orynbayeva, Z.; Friedman, G.; Gogotsi, Y. Nanoprobes for intracellular and single cell surface-enhanced Raman spectroscopy (SERS). *J. Raman Spectrosc.* **2012**, *43* (7), 817−827.
(27) Jarvis, R. M.; Law, N.; Shadi, I. T.; O'Brien, P.; Lloyd, J. R.; Goodacre, R. Surface-enhanced Raman scattering from intracellular and extracellular bacterial locations. *Anal. Chem.* **2008**, *80* (17), 6741−6746.
(28) Shamsaie, A.; Jonczyk, M.; Sturgis, J.; Robinson, J. P.; Irudayaraj, J. Intracellularly grown gold nanoparticles as potential surface-enhanced Raman scattering probes. *J. Biomed. Opt.* **2007**, *12* (2), 020502.
(29) Huang, H.; Chen, W.; Pan, J.; Chen, Q.; Feng, S.; Yu, Y.; Chen, Y.; Su, Y.; Chen, R. SERS spectra of a single nasopharyngeal carcinoma cell based on intracellularly grown and passive uptake Au nanoparticles. *Spectroscopy* **2011**, *26* (3), 187−194.
(30) Liu, Z.; Hu, C.; Li, S.; Zhang, W.; Guo, Z. Rapid intracellular growth of gold nanostructures assisted by functionalized graphene oxide and its application for surface-enhanced Raman spectroscopy. *Anal. Chem.* **2012**, *84* (23), 10338−10344.
(31) *Test No. 201: Freshwater Alga and Cyanobacteria, Growth Inhibition Test*; OECD Publishing: Paris, 2011.
(32) Frens, G. Controlled nucletion for the regulation of the particle size in monodiperse gold suspensions. *Nature, Phys. Sci.* **1973**, *241*, 20−22.
(33) Lowe, K. TEM Training and Sample Processing at the Virginia-Maryland Regional College of Veterinary Medicine Morphology Service Laboratory. Blacksburg, VA, 2012.
(34) *Spurr Low-Viscosity Embedding Media*; Technical Data Sheet 127; Polysciences, Inc.: Warrington, PA, 2010.
(35) Spurr, A. R. A low-viscosity epoxy resin embedding medium for electron microscopy. *J. Ultrastruct. Res.* **1969**, *26* (1−2), 31−43.
(36) Daniel, M.-C.; Astruc, D. Gold nanoparticles: Assembly, supramolecular chemistry, quantum-size-related properties, and applications toward biology, catalysis, and nanotechnology. *Chem. Rev.* **2003**, *104* (1), 293−346.
(37) Ahmad, A.; Senapati, S.; Khan, M. I.; Kumar, R.; Ramani, R.; Srinivas, V.; Sastry, M. Intracellular synthesis of gold nanoparticles by a novel alkalotolerant actinomycete, *Rhodococcus* species. *Nanotechnology* **2003**, *14* (7), 824.
(38) Belazi, D.; Solé-Domènech, S.; Johansson, B.; Schalling, M.; Sjövall, P. Chemical analysis of osmium tetroxide staining in adipose tissue using imaging ToF-SIMS. *Histochem. Cell Biol.* **2009**, *132* (1), 105−115.
(39) Pearman, W. F.; Fountain, A. W. Classification of chemical and biological warfare agent simulants by surface-enhanced Raman spectroscopy and multivariate statistical techniques. *Appl. Spectrosc.* **2006**, *60*, 356−365.
(40) Gelder, J. D.; Gussem, K. D.; Vandenabeele, P.; Moens, L. Reference database of Raman spectra of biological molecules. *J. Raman Spectrosc.* **2007**, *38* (9), 1133−1147.
(41) Movasaghi, Z.; Rehman, S.; Rehman, I. U. Raman spectroscopy of biological tissues. *Appl. Spectrosc. Rev.* **2007**, *42* (5), 493−541.
(42) Grow, A. E. Label-Free Fingerprinting of Pathogens by Raman Spectroscopy Techniques. In *Principles of Bacterial Detection: Biosensors, Recognition Receptors and Microsystems*; Zourob, M.; Elwary, S.; Turner, A., Eds.; Springer: New York, 2008; pp 525−566.
(43) Halvorson, R. A.; Leng, W.; Vikesland, P. J. Differentiation of microcystin, nodularin, and their component amino acids by drop-coating deposition Raman spectroscopy. *Anal. Chem.* **2011**, *83* (24), 9273−9280.
(44) Muntean, C. M.; Leopold, N.; Halmagyi, A.; Valimareanu, S. Surface-enhanced Raman scattering assessment of DNA from leaf tissues adsorbed on silver colloidal nanoparticles. *J. Raman Spectrosc.* **2013**, *44* (6), 817−822.
(45) Chan, J. W.; Taylor, D. S.; Zwerdling, T.; Lane, S. M.; Ihara, K.; Huser, T. Micro-Raman spectroscopy detects individual neoplastic and normal hematopoietic cells. *Biophys. J.* **2006**, *90* (2), 648−656.
(46) Kuznetsova, S.; Knaff, D. B.; Hirasawa, M.; Sétif, P.; Mattioli, T. A. Reactions of spinach nitrite reductase with its substrate, nitrite, and a putative intermediate, hydroxylamine. *Biochemistry (Mosc)* **2004**, *43* (33), 10765−10774.
(47) Ondrias, M. R.; Carson, S. D.; Hirasawa, M.; Knaff, D. B. Characterization of the siroheme active site in spinach nitrite reductase by resonance Raman spectroscopy. *Biochim. Biophys. Acta, Protein Struct. Mol. Enzymol.* **1985**, *830* (2), 159−163.
(48) Dooley, D. M.; Moog, R. S.; Liu, M. Y.; Payne, W. J.; LeGall, J. Resonance Raman spectra of the copper-sulfur chromophores in *Achromobacter cycloclastes* nitrite reductase. *J. Biol. Chem.* **1988**, *263* (29), 14625−14628.
(49) Chowdhury, J.; Ghosh, M.; Mukherjee, K. M.; Misra, T. N. pH dependent surface enhanced Raman scattering of molecules adsorbed on silver hydrosol. *Internet J. Vib. Spectrosc.* **2000**, *4* (2), 7.
(50) Deckert-Gaudig, T.; Bailo, E.; Deckert, V. Tip-enhanced Raman scattering (TERS) of oxidised glutathione on an ultraflat gold nanoplate. *Phys. Chem. Chem. Phys.* **2009**, *11* (34), 7360−7362.
(51) Huong, P. V. Metallo-Organic Complexes and Carcinogenesis. In *Molecules in Physics, Chemistry and Biology: Molecular Phenomena in Biological Sciences*; Maruani, J., Ed.; Kluwer Academic Publishers: Dordrecht, The Netherlands, 1989; pp 87−109.
(52) Xiao, Y.-J.; Chen, Y.-F.; Gao, X.-X. Comparative study of the surface enhanced near infrared Raman spectra of adenine and nad+ on a gold electrode. *Spectrochim. Acta, Part A* **1999**, *55* (6), 1209−1218.
(53) Xiao, Y.-J.; Wang, T.; Wang, X.-Q.; Gao, X.-X. Surface-enhanced near-infrared Raman spectroscopy of nicotinamide adenine dinucleotides on a gold electrode. *J. Electroanal. Chem.* **1997**, *433* (1−2), 49−56.
(54) Zheng, J.; Chen, Y. Q.; Callender, R. A study of the binding of nadp coenzymes to dihydrofolate reductase by Raman difference spectroscopy. *Eur. J. Biochem.* **1993**, *215* (1), 9−16.
(55) Chen, D.; Yue, K. T.; Martin, C.; Rhee, K. W.; Sloan, D.; Callender, R. Classical Raman spectroscopic studies of nadh and nad+ bound to liver alcohol dehydrogenase by difference techniques. *Biochemistry (Mosc)* **1987**, *26* (15), 4776−4784.
(56) Austin, J. C.; Hester, R. E. Surface-enhanced Raman spectroscopy of nad+ and related compounds. *J. Chem. Soc., Faraday Trans. 1* **1989**, *85* (5), 1159−1168.
(57) Huang, Y. Y.; Beal, C. M.; Cai, W. W.; Ruoff, R. S.; Terentjev, E. M. Micro-Raman spectroscopy of algae: Composition analysis and fluorescence background behavior. *Biotechnol. Bioeng.* **2010**, *105* (5), 889−898.
(58) Wood, B. R.; Heraud, P.; Stojkovic, S.; Morrison, D.; Beardall, J.; McNaughton, D. A portable Raman acoustic levitation spectroscopic system for the identification and environmental monitoring of algal cells. *Anal. Chem.* **2005**, *77* (15), 4955−4961.
(59) Sengupta, A.; Mujacic, M.; Davis, E. Detection of bacteria by surface-enhanced Raman spectroscopy. *Anal. Bioanal. Chem.* **2006**, *386* (5), 1379−1386.
(60) Zeiri, L.; Bronk, B. V.; Shabtai, Y.; Eichler, J.; Efrima, S. Surface-enhanced Raman spectroscopy as a tool for probing specific biochemical components in bacteria. *Appl. Spectrosc.* **2004**, *58* (1), 33−40.

(61) Bossuyt, B. T. A.; Janssen, C. R. Long-term acclimation of *Pseudokirchneriella subcapitata* (korshikov) hindak to different copper concentrations: Changes in tolerance and physiology. *Aquat. Toxicol.* **2004**, *68* (1), 61−74.
(62) Gao, P.; Weaver, M. J. Surface-enhanced Raman spectroscopy as a probe of adsorbate-surface bonding: Benzene and monosubstituted benzenes adsorbed at gold electrodes. *J. Phys. Chem.* **1985**, *89* (23), 5040−5046.
(63) Gao, P.; Weaver, M. J. Metal-adsorbate vibrational frequencies as a probe of surface bonding: Halides and pseudohalides at gold electrodes. *J. Phys. Chem.* **1986**, *90* (17), 4057−4063.
(64) Bozzini, B.; Romanello, V.; Mele, C. A SERS investigation of the electrodeposition of Au in a phosphate solution. *Surf. Coat. Technol.* **2007**, *201* (14), 6267−6272.
(65) Joo, S. W.; Han, S. W.; Kim, K. Adsorption characteristics of 1,3-propanedithiol on gold: Surface-enhanced Raman scattering and ellipsometry study. *J. Phys. Chem. B* **2000**, *104* (26), 6218−6224.
(66) Bjerneld, E. J.; Johansson, P.; Käll, M. Single molecule vibrational fine-structure of tyrosine adsorbed on Ag nano-crystals. *Single Mol.* **2000**, *1* (3), 239−248.
(67) Kumar, S. A.; Abyaneh, M. K.; Gosavi, S. W.; Kulkarni, S. K.; Ahmad, A.; Khan, M. I. Sulfite reductase-mediated synthesis of gold nanoparticles capped with phytochelatin. *Biotechnol. Appl. Biochem.* **2007**, *047* (4), 191−195.
(68) Prasad, M. N. V. *Metals in the Environment: Analysis by Biodiversity*; Marcel Dekker: New York, 2001.
(69) Gala, W. R.; Giesy, J. P. Using the carotenoid biosynthesis inhibiting herbicide, fluridone, to investigate the ability of carotenoid pigments to protect algae from the photo-induced toxicity of anthracene. *Aquat. Toxicol.* **1993**, *27*, 61−70.
(70) Zhang, Y. X.; Zheng, J.; Gao, G.; Kong, Y. F.; Zhi, X.; Wang, K.; Zhang, X. Q.; Cui, D. X. Biosynthesis of gold nanoparticles using chloroplasts. *Int. J. Nanomed.* **2011**, *6*, 2899−2906.
(71) Barazzouk, S.; Bekale, L.; Hotchandani, S. Enhanced photostability of chlorophyll-*a* using gold nanoparticles as an efficient photoprotector. *J. Mater. Chem.* **2012**, *22* (48), 25316−25324.
(72) Mukherjee, P.; Roy, M.; Mandal, B. P.; Dey, G. K.; Mukherjee, P. K.; Ghatak, J.; Tyagi, A. K.; Kale, S. P. Green synthesis of highly stabilized nanocrystalline silver particles by a non-pathogenic and agriculturally important fungus *T. asperellum*. . *Nanotechnology* **2008**, *19*, 075103.
(73) Ma, X.; Geiser-Lee, J.; Deng, Y.; Kolmakov, A. Interactions between engineered nanoparticles (ENPs) and plants: Phytotoxicity, uptake and accumulation. *Sci. Total Environ.* **2010**, *408* (16), 3053−3061.
(74) Bantz, K. C.; Meyer, A. F.; Wittenberg, N. J.; Im, H.; Kurtuluş, Ö.; Lee, S. H.; Lindquist, N. C.; Oh, S.-H.; Haynes, C. L. Recent progress in SERS biosensing. *Phys. Chem. Chem. Phys.* **2011**, *13* (24), 11551−11567.
(75) Nath, S.; Ghosh, S. K.; Kundu, S.; Praharaj, S.; Panigrahi, S.; Pal, T. Is gold really softer than silver? Hsab principle revisited. *J. Nanopart. Res.* **2006**, *8* (1), 111−116.
(76) Quester, K.; Avalos-Borja, M.; Vilchis-Nestor, A. R.; Camacho-López, M. A.; Castro-Longoria, E. SERS properties of different sized and shaped gold nanoparticles biosynthesized under different environmental conditions by *Neurospora crassa* extract. *PLoS One* **2013**, *8* (10), e77486.